Research Article | Vol. 25, No. 2 | 23 Jan 2017 | OPTICS EXPRESS 1030

Optics EXPRESS

High resolution fluorescence bio-imaging upconversion nanoparticles in insects

MASFER ALKAHTANI,[1,2,8] YUNYUN CHEN,[3,4,8] JULIE J. PEDRAZA,[5] JORGE M. GONZÁLEZ,[5] DILWORTH Y. PARKINSON,[6] PHILIP R. HEMMER,[1,7] AND HONG LIANG[3,4,*]

[1]*Institute for Quantum Science and Engineering (IQSE) and Department of Physics and Astronomy, Texas A&M University, College Station, TX 77843-4242, USA*
[2]*The National Center for Applied Physics, KACST, P.O. Box 6086, Riyadh 11442, Saudi Arabia*
[3]*Materials Science and Engineering, Texas A&M University, College Station, Texas 77843, USA*
[4]*Mechanical Engineering, Texas A&M University, College Station, Texas 77843, USA*
[5]*Department of Plant Science, California State University, Fresno, California 93740, USA*
[6]*Advanced Light Source, Lawrence Berkeley National Laboratory, Berkeley, California 94720, USA*
[7]*Electrical & Computer Engineering Department, Texas A&M University, College Station, TX 77843-3128, USA*
[8]*These authors contributed equally to this work*
[*]*hliang@tamu.edu*

Abstract: Imaging fluorescent markers with brightness, photostability, and continuous emission with auto fluorescence background suppression in biological samples has always been challenging due to limitations of available and economical techniques. Here we report a new approach, to achieve high contrast imaging inside small and difficult biological systems with special geometry such as fire ants, an important agricultural pest, using a homemade cost-effective optical system. Unlike the commonly used rare-earth doped fluoride nanoparticles, we utilized nanoparticles with a high upconversion efficiency in water. Specifically $Y_2O_3 : Er^{+3}, Yb^{+3}$ nanoparticles (40-50 nm diameter) were fed to fire ants as food and then a simple illuminating experiment was conducted at 980 nm wavelength at relatively low pump intensity $8\ kW.cm^{-2}$. The locations were further confirmed by X-ray tomography, where most particles aggregated inside the ant's mouth. High resolution, fast, and economical optical imaging system opens the door for studying more complex biological systems.

OCIS codes: (110.0110) Imaging systems; (110.2970) Image detection systems.

References and links

1. X. Michalet, F. F. Pinaud, L. A. Bentolila, J. M. Tsay, S. Doose, J. J. Li, G. Sundaresan, A. M. Wu, S. S. Gambhir, and S. Weiss, "Quantum dots for live cells, in vivo imaging, and diagnostics," Science **307**(5709), 538–544 (2005).
2. M. Haase and H. Schäfer, "Upconverting nanoparticles," Angew. Chem. Int. Ed. Engl. **50**(26), 5808–5829 (2011).
3. X. Huang, "Broadband dye-sensitized upconversion: A promising new platform for future solar upconverter design," J. Alloys Compd. **690**, 356–359 (2017).
4. Q. le Masne de Chermont, C. Chanéac, J. Seguin, F. Pellé, S. Maîtrejean, J. P. Jolivet, D. Gourier, M. Bessodes, and D. Scherman, "Nanoprobes with near-infrared persistent luminescence for in vivo imaging," Proc. Natl. Acad. Sci. U.S.A. **104**(22), 9266–9271 (2007).
5. G. Mialon, S. Türkcan, G. Dantelle, D. P. Collins, M. Hadjipanayi, R. A. Taylor, T. Gacoin, A. Alexandrou, and J.-P. Boilot, "High Up-Conversion Efficiency of YVO4:Yb,Er Nanoparticles in Water down to the Single-Particle Level," J. Phys. Chem. C **114**(51), 22449–22454 (2010).
6. D. R. Larson, W. R. Zipfel, R. M. Williams, S. W. Clark, M. P. Bruchez, F. W. Wise, and W. W. Webb, "Water-soluble quantum dots for multiphoton fluorescence imaging in vivo," Science **300**(5624), 1434–1436 (2003).
7. W. R. Zipfel, R. M. Williams, and W. W. Webb, "Nonlinear magic: multiphoton microscopy in the biosciences," Nat. Biotechnol. **21**(11), 1369–1377 (2003).
8. D. J. Gargas, E. M. Chan, A. D. Ostrowski, S. Aloni, M. V. P. Altoe, E. S. Barnard, B. Sanii, J. J. Urban, D. J. Milliron, B. E. Cohen, and P. J. Schuck, "Engineering bright sub-10-nm upconverting nanocrystals for single-molecule imaging," Nat Nano **9**(4), 300–305 (2014).

#278933 http://dx.doi.org/10.1364/OE.25.001030
Journal © 2017 Received 17 Oct 2016; revised 25 Nov 2016; accepted 25 Nov 2016; published 12 Jan 2017

Optics EXPRESS

9. F. Zhang, "Surface Modification and Bioconjugation of Upconversion Nanoparticles," in *Photon Upconversion Nanomaterials* (Springer Berlin Heidelberg, Berlin, Heidelberg, 2015), pp. 159–185.
10. U. Resch-Genger, M. Grabolle, S. Cavaliere-Jaricot, R. Nitschke, and T. Nann, "Quantum dots versus organic dyes as fluorescent labels," Nat. Methods **5**(9), 763–775 (2008).
11. T. Taniguchi, K. Soga, K. Tokuzen, K. Tsujiuchi, T. Kidokoro, K. Tomita, K.-i. Katsumata, N. Matsushita, and K. Okada, "NIR-excited NIR and visible luminescent properties of amphipathic YVO4: Er3+/Yb3+ nanoparticles," J. Mater. Sci. **47**(5), 2241–2247 (2012).
12. C. T. Xu, Q. Zhan, H. Liu, G. Somesfalean, J. Qian, S. He, and S. Andersson-Engels, "Upconverting nanoparticles for pre-clinical diffuse optical imaging, microscopy and sensing: Current trends and future challenges," Laser Photonics Rev. **7**(5), 663–697 (2013).
13. X. Huang, "Enhancement of near-infrared to near-infrared upconversion luminescence in sub-10-nm ultra-small LaF(3):Yb(3+)/Tm(3+) nanoparticles through lanthanide doping," Opt. Lett. **40**(22), 5231–5234 (2015).
14. X. Huang, "Giant enhancement of upconversion emission in ($NaYF_4$:Nd^{3+}/Yb^{3+}/Ho^{3+})/($NaYF_4$:Nd^{3+}/Yb^{3+}) core/shell nanoparticles excited at 808 nm," Opt. Lett. **40**(15), 3599–3602 (2015).
15. G. Chen, H. Qiu, P. N. Prasad, and X. Chen, "Upconversion nanoparticles: design, nanochemistry, and applications in theranostics," Chem. Rev. **114**(10), 5161–5214 (2014).
16. J. Chen and J. X. Zhao, "Upconversion nanomaterials: synthesis, mechanism, and applications in sensing," Sensors (Basel) **12**(3), 2414–2435 (2012).
17. Y. Liu, K. Ai, J. Liu, Q. Yuan, Y. He, and L. Lu, "A high-performance ytterbium-based nanoparticulate contrast agent for in vivo X-ray computed tomography imaging," Angew. Chem. Int. Ed. Engl. **51**(6), 1437–1442 (2012).
18. S.-B. Yu and A. D. Watson, "Metal-Based X-ray Contrast Media," Chem. Rev. **99**(9), 2353–2378 (1999).
19. S. Zeng, H. Wang, W. Lu, Z. Yi, L. Rao, H. Liu, and J. Hao, "Dual-modal upconversion fluorescent/X-ray imaging using ligand-free hexagonal phase NaLuF4:Gd/Yb/Er nanorods for blood vessel visualization," Biomaterials **35**(9), 2934–2941 (2014).
20. J. C. Boyer and F. C. van Veggel, "Absolute quantum yield measurements of colloidal NaYF4: Er3+, Yb3+ upconverting nanoparticles," Nanoscale **2**(8), 1417–1419 (2010).
21. S. S. H. Tahira Gul, F. Zafar Ahmad Khan, and S. Amir Manzoor, "Potential of Nanotechnology in Agriculture and Crop Protection: A Review," Applied Sciences and Business Economics **1**, 3–8 (2014).
22. S. S. Mukhopadhyay, "Nanotechnology in agriculture: prospects and constraints," Nanotechnol. Sci. Appl. **7**, 63–71 (2014).
23. Y. Chen, C. Sanchez, Y. Yue, J. M. González, D. Y. Parkinson, and H. Liang, "Observation of two-dimensional yttrium oxide nanoparticles in mealworm beetles (Tenebrio molitor)," J. Synchrotron Radiat. **23**(5), 1197–1201 (2016).
24. L. Diez, L. Urbain, P. Lejeune, and C. Detrain, "Emergency measures: Adaptive response to pathogen intrusion in the ant nest," Behav. Processes **116**, 80–86 (2015).
25. A. Rocha, Y. Zhou, S. Kundu, J. M. González, S. BradleighVinson, and H. Liang, "In vivo observation of gold nanoparticles in the central nervous system of Blaberus discoidalis," J. Nanobiotechnology **9**(1), 5 (2011).
26. X. Li, F. Zhang, and D. Zhao, "Highly efficient lanthanide upconverting nanomaterials: Progresses and challenges," Nano Today **8**(6), 643–676 (2013).
27. F. Auzel, "Upconversion and anti-Stokes processes with f and d ions in solids," Chem. Rev. **104**(1), 139–174 (2004).
28. W. Chen, C. Shi, T. Tao, M. Ji, S. Zheng, X. Sang, X. Liu, and J. Qiu, "Optical temperature sensing with minimized heating effect using core-shell upconversion nanoparticles," RSC Advances **6**(26), 21540–21545 (2016).
29. G. Jiang, S. Zhou, X. Wei, Y. Chen, C. Duan, M. Yin, B. Yang, and W. Cao, "794 nm excited core-shell upconversion nanoparticles for optical temperature sensing," RSC Advances **6**(14), 11795–11801 (2016).
30. X. Zhu, W. Feng, J. Chang, Y.-W. Tan, J. Li, M. Chen, Y. Sun, and F. Li, "Temperature-feedback upconversion nanocomposite for accurate photothermal therapy at facile temperature," Nat. Commun. **7**, 10437 (2016).
31. Y. Chen, C. Sanchez, Y. Yue, M. de Almeida, J. M. González, D. Y. Parkinson, and H. Liang, "Observation of yttrium oxide nanoparticles in cabbage (Brassica oleracea) through dual energy K-edge subtraction imaging," J. Nanobiotechnology **14**(1), 23 (2016).

1. Introduction

Over the past decades, intensive efforts have been focused to develop effective nanoparticles like fluorescent markers in biological imaging [1–3]. Most of the traditional fluorescent markers such as organic dyes and quantum dots exhibit high luminesce efficiency within the visible range when stimulated by high-energy lasers excitation. However their high-energy illumination causes the surrounding biological samples to emit light in the visible window, resulting in a significant auto-fluorescence which will reduces the sensitivity of using these fluorescent markers in deep tissue imaging [4, 5]. Enormous efforts have been made to overcome these autofluoresence limitations [6, 7]. Photoluminescence process in organic dyes and quantum dots have been found to be one of the best candidate solutions for the

Optics EXPRESS

autofluoresence issues as bio-fluorescent markers in the biological tissues transparency window. Most of the upconversion fluorescent markers systems including upconversion organic dyes and quantum dots require high laser excitation intensity (typically~$10^7 - 10^{11}$ W.cm^{-2}), often resulting in serious damage of biological samples [8, 9]. Furthermore, upconversion organic dyes and quantum dot are also limited by photobleating, blinking, and toxicity [10].

Lanthanide ions $Ln^{+3}(Ln = Er, Tm, Ho, etc.)$ doped upconversion nanocrystals (UCNPs) have been found to overcome many of the previous drawbacks of the upconversion organic dyes and quantum dots [11–14]. The upconverting process of these UCNPs is based on sequential near-infrared photons absorption (excited states absorption) [15] enhanced by energy transfer from Yb ions, resulting in a desired luminescence emitted in a visible range. Due to long-lifetime in their metastable states (microsecond scale) [16] the intensity thresholds are the lowest of all upconversion emitters. These advantages make them more efficient compared to upconversion organic dyes and quantum dot. In addition, UCNPs also have shown high-contrast in x-ray imaging due to their large x-ray absorption coefficient [17–19]. Therefore, UCNPs can be used to accomplish fast and cheap optical bio-imaging whose absolute accuracy can be directly validated with x-ray imaging when desired.

To date, the commonly used upconversion nanoparticles $NaYF_4 : Er^{+3}, Yb^{+3}$ have been proposed to be one of the best upconversion nanoparticles due to their strong upconversion luminescence (UCL) and relatively good quantum efficiency when despised in organic solvent such as hexanes. However, their UCL and quantum efficiency drops when dispersed in water [8, 20].Therefore they are not favorable in bioimaging application since water is the main concern in biological samples.

In the present research, southern fire ants (Solenopsis xyloni, Formicidae) were selected due to their importance in agriculture. To date, there was no alternative to effectively eliminate them from critical areas. Imaging upconversion nanoparticles could be included as a method to understand fire ants by study their habits and interactions. This would help for future work to find effective ways to definitively control such nuisance [21, 22].

In this work, we synthesized water-based and highly crystalline $Y_2O_3 : Er^{+3}, Yb^{+3}$ nanoparticles as our fluorescent and x-ray bio-probes in this experiment with an estimated size range of ~40-50 nm. These nanoparticles were fed to fire ants as our biological model. We performed X-ray and UC fluorescent bioimaging of $Y_2O_3 : Er^{+3}, Yb^{+3}$ nanoparticles inside an ant's body using a relatively low excitation intensity of 8 kW.cm^{-2} at 980 nm in confocal scanning microscope setup and X-ray sources. We were able to clearly detect the upconversion luminescence emission and x-ray signals of $Y_2O_3 : Er^{+3}, Yb^{+3}$ nanoparticles inside ants which make these UCNPs multi-modal bio-probes.

2. Methods

2.1 Characterizations of $Y_2O_3 : Er^{+3}, Yb^{+3}$ upconversion nanoparticles

The synthesis of $\mathbf{Y_2O_3 : Er^{+3}, Yb^{+3}}$ NPs was reported in our previous work [23]. The crystal structure of as-synthesized NPs was determined by advance X-ray diffractometer (Bruker) conducting at 40 kV, 40 mA. The transmission electron microscope (TEM, JEOL 1200 EX) and high resolution TEM (JEOL 1200 EX) were used to indicate the morphology of as-synthesized NPs at both low and high resolution.

2.2 $Y_2O_3 : Er^{+3}, Yb^{+3}$ NPs exposure and fed-ant samples

From a colony of agriculturally damaging southern fire ants (Solenopsis xyloni) kept at room temperature (25 °C) and in a 12:12 h Light:Dark cycle, in the Entomology Laboratory, at

Optics EXPRESS

California State University, Fresno, CA, individuals were extracted for experimentation. Isolated southern fire ants were placed in polystyrene boxes with sides covered with fluon to avoid their scape. In a first test, one group of southern fire ants was fed with a 10% honey-water + NPs solution at libitum, while a control group was fed only with 10% honey-water Fig. 1(a). Since fire ants are recognized carnivorous insects, while contained in polystyrene boxes with fluon covered sides, another group was fed with mealworms previously fed with 10% Honey-water + NPs and positively tested for internal presence of NPs [23], while a control group of southern fire ants was fed with mealworms fed with 10% honey-water only Fig. 1(b). Micro-tomography imaging failed to detect NPs inside the digestive track and the coelom of the tested individuals fed with NPs in the 10% Honey-water diet. However, NPs could be clearly seen within the buccal cavity (Fig. 5). As previous research on social ants seems to suggest [24] hygiene and grooming behavior of fire ants might help to isolate foreign objects from their food not allowing them to be ingested which might explain that no NPs were found in other regions of the digestive system, except for the mouth. If we had been able to find NPs inside the coelom or other parts of the body, we would have expected them to be encapsulated by hemocytes as previous experiences indicate [23, 25].

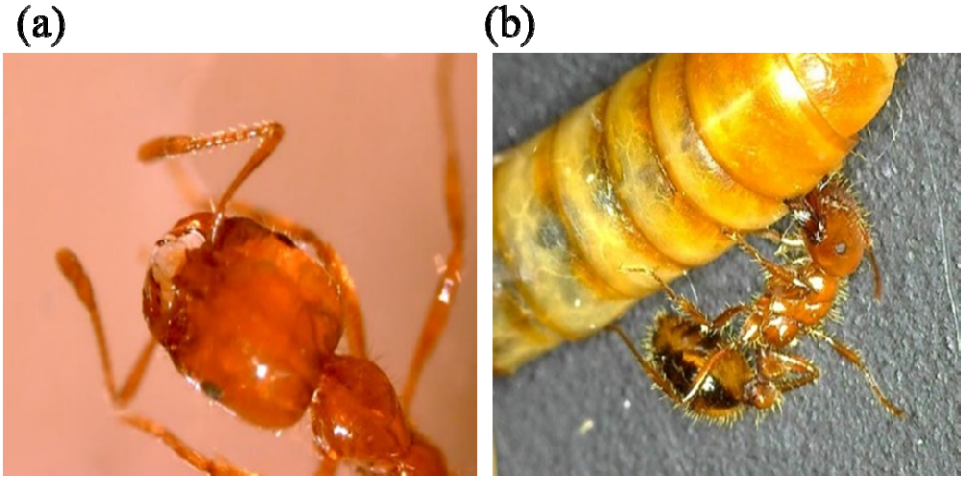

Fig. 1. Southern fire ant feeding: (a) on a solution of Honey and water provided at libitum; (b) from a mealworm previously fed with $\mathbf{Y_2O_3:Er^{+3},Yb^{+3}}$ NPs.

2.3 Confocal scanning microscopy setup

In this experiment we used a confocal laser scanning microscopy equipped with a 10x, NA = 0.26 mitutoyo microscope objective. Two fire ant specimens were fed with a solution containing $\mathbf{Y_2O_3:Er^{+3},Yb^{+3}}$ UCNPs, and placed on a glass coverslip, were they were excited with 980nm laser source filtered by a short-pass filter (800 SP) (Fig. 2). The laser intensity was $8\mathbf{kW.cm^{-2}}$. The UCL was collected with a homemade spectrometer equipped with a starlight camera (Trius camera model SX-674). Two dimensional Images scanned with a galvoscanner were recorded using a photon counter (Hamamatsu photon counter model number H7155-21) as shown in Figs. 5(a) and 5(b). Compared to typical costly commercial imaging systems, the main advantage of this system, it can be modified and accessible efficiently for further research investigations in this imaging field or other related projects without restrictions. Furthermore, this homemade imaging system is cheap and fast to be built from scratch for limited funding research groups.

Optics EXPRESS

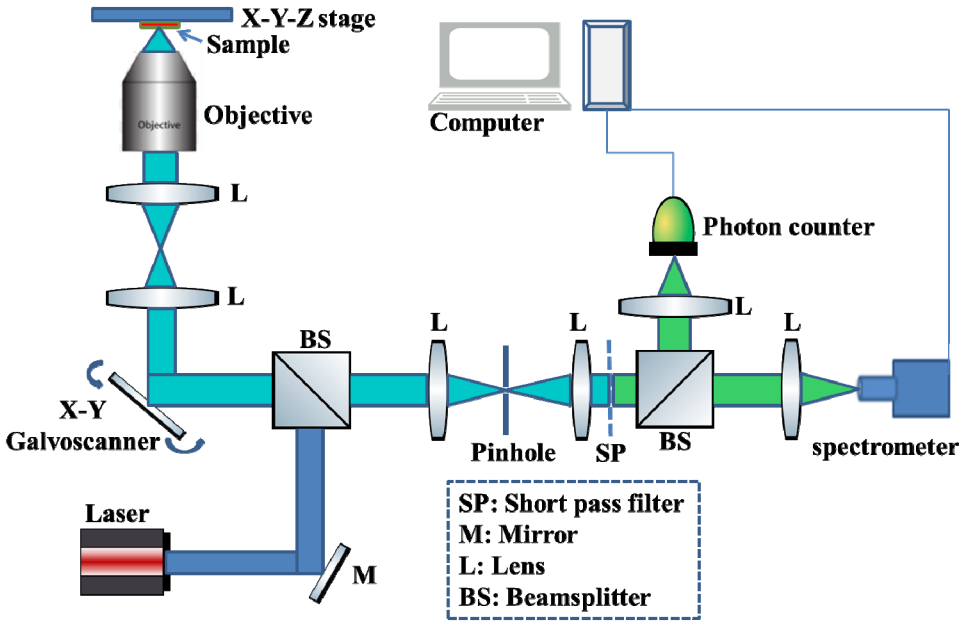

Fig. 2. Schematic drawing of a confocal laser scanning microscope setup consisting of a 4f imaging system, a photon counter, and a spectrometer.

3. Results and discussion

3.1 Upconversion emission of $Y_2O_3:Er^{+3},Yb^{+3}$ nanoparticles in water

The visible upconversion emission of $Y_2O_3:Er^{+3},Yb^{+3}$ nanoparticles under 980 nm excitation can be illustrated as shown in Fig. 3(a). The $Y_2O_3:Er^{+3},Yb^{+3}$ nanoparticles spin coated onto a microscope coverslip and covered with a water droplet, were placed in a confocal scanning microscope as shown in (Fig. 2). The nanoparticles were excited with 980nm laser source filtered by a short-pass filter (800 SP). The laser intensity was varied from (0.5- 8) $kW.cm^{-2}$ The corresponding upconversion luminescence spectra (UCL) with strong green emission centered at 550nm and weak red emission centered at 650nm were collected with a homemade spectrometer equipped with a starlight camera (Trius camera model SX-674) and presented in Fig. 3(c). The $Y_2O_3:Er^{+3},Yb^{+3}$ upconversion nanoparticles revealed higher quantum efficiency (1.2%) under water droplet under 980 nm illumination compared to the commonly used $NaYF_4:Er^{+3},Yb^{+3}$ UCNPs. The quantum efficiency of the latter dropped to almost 0% and became undetectable UC luminescence when covered by water droplet, especially for small size around (40 nm average size).

In order to fully understand the upconversion emission spectrum, we will discuss the physics behind this unique upconversion process of $Y_2O_3:Er^{+3},Yb^{+3}$ nanoparticles. Among the lanthanides ions, we choose erbium Er^{+3} ion to provide the upconversion luminescence under 980 nm laser excitation, however the erbium Er^{+3} ion has a weak absorption cross section at that excitation wavelength [26]. To overcome this limitation, we consider the energy transfer upconversion (ETU), in which ytterbium ion (Yb^{+3}) is used as a sensitizer to the erbium Er^{+3} ion owing to its very high absorption cross section at 980 nm. As a result, ytterbium ion (Yb^{+3}) can efficiently transfer its excitation Er^{+3} ion [27] using the ETU process according to the following transition:

Optics EXPRESS

$$(^4I_{15/2})Er^{+3} + (^2F_{5/2})\ Yb^{+3} \rightarrow (^4I_{11/2})Er^{+3} + (^2F_{7/2})\ Yb^{+3}$$

Consequently, as shown in Fig. 3(b), the first NIR photon absorption of 980 nm laser excitation excites the synthesizer Yb^{+3} ion to its $(^2F_{5/2})$ excited state. The energy transfer from the $(^2F_{5/2})Yb^{+3}$ excited state promotes Er^{+3} to its quasi-resonance metastable state $^4I_{15/2}$. A second NIR photon absorption by Yb^{+3} populates its $(^2F_{5/2})$ excited state and energy transfer further excites the Er^{+3} $(^4I_{15/2})$ metastable state to a high energy excited $(^4F_{7/2})Er^{+3}$ state, followed by nonradiative relaxations to $(^2H_{11/2}, {}^4S_{3/2}$, and $^4F_{9/2})Er^{+3}$ states throughout the multi-phonon relaxations. Two main green emissions (520 nm and 550 nm) arise from radiative transitions which occur from $^2H_{11/2}, {}^4S_{3/2}$ states to the ground state $^4I_{15/2}$. In addition, another red emission centered at 650 nm corresponding to this transition: $^4F_{9/2} \rightarrow {}^4I_{15/2}$.

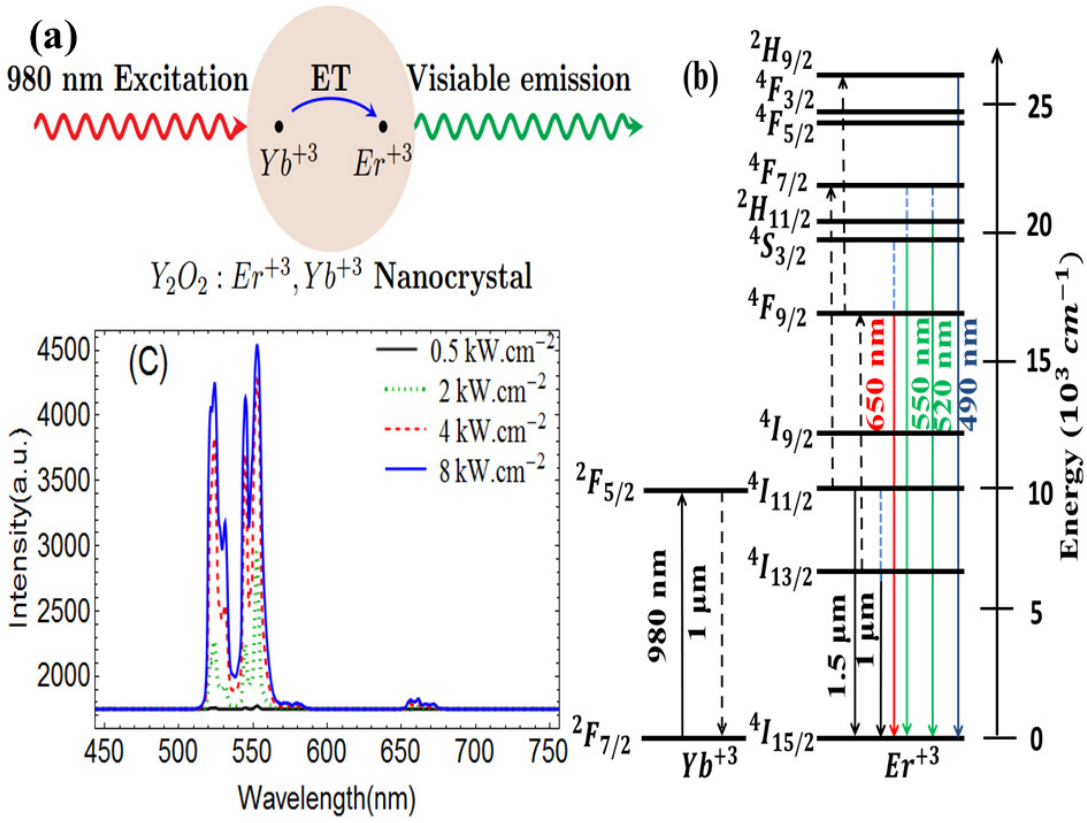

Fig. 3. (a) A schematic illustration of $Y_2O_3 : Er^{+3}, Yb^{+3}$ upconversion nanoparticles under 980 nm laser excitation. (b) A Schematic drawing of energy transfer mechanism between Er^{+3} and Yb^{+3}. Curved dashed, straight dashed and full arrows represent energy transfer, multi-phonon relaxation, and radiative emission process, respectively [5]. (c) Upconversion luminescence spectra of 1wt% of $Y_2O_3 : Er^{+3}, Yb^{+3}$ upconversion nanoparticles spin coated on cover slip and covered by a droplet of water under 980 nm laser excitation at different laser powers.

3.2 TEM image and particle size measurements of $Y_2O_3:Er^{+3},Yb^{+3}$ nanoparticles

High magnification imaging was performed on $Y_2O_3:Er^{+3},Yb^{+3}$ nanoparticles in order to visualize crystal structure of the nanoparticles. Figure 4(a) illustrates high crystalline $Y_2O_3:Er^{+3},Yb^{+3}$ nanoparticles which expected to reveal a strong upconversion luminescence. Figure 4(b) shows a distribution of the UCNPs peaked at (40-50nm) particle size corresponding to that shown in Fig. 4(a). The particle size was recorded using Dynamic Light Scattering (DLS) system (Malvern Instruments) equipped with 50 mW, 660 nm red laser.

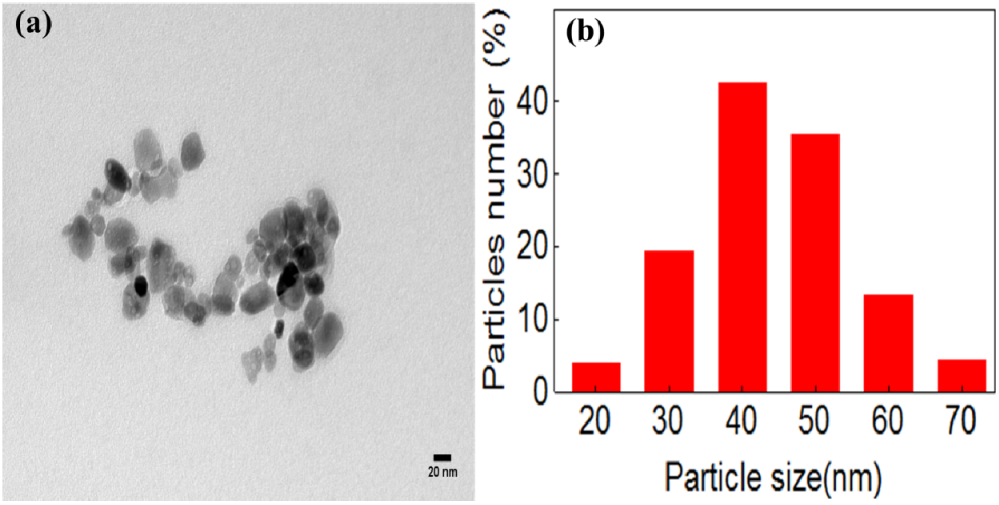

Fig. 4. (a) A high magnification TEM image of $Y_2O_3:Er^{+3},Yb^{+3}$ upconversion nanoparticles dissolved in water and droped on a TEM grid. (b) A particle size distribution of 1mg/ml of $Y_2O_3:Er^{+3},Yb^{+3}$ upconversion nanoparticles taken by (DLS).

3.3 Optical imaging of $Y_2O_3:Er^{+3},Yb^{+3}$ upconversion nanoparticles as bio-probe inside fire ants

The primary goal of this experiment was to obtain high-contrast images of $Y_2O_3:Er^{+3},Yb^{+3}$ upconversion nanoparticles as bio-probe inside fire ants using economical and homemade optical system. From a laboratory colony of southern fire ants (Solenopsis xyloni), several individuals were extracted, isolated and fed with $Y_2O_3:Er^{+3},Yb^{+3}$ upconversion nanoparticles as explained in detail in the Methods section. Optical images of the fire ants were carried out by using a homemade confocal scanning microscope. The fire ant specimens were placed on a glass coverslip on top of 10x, NA = 0.26 mitutoyo microscope objective, where they were excited with a 980nm laser illumination source filtered by a short-pass filter (800 SP). The laser intensity was 8) $kW.cm^{-2}$ High contrast images of $Y_2O_3:Er^{+3},Yb^{+3}$ upconversion nanoparticles (red spots) inside the mouth of fire ants as shown in Figs. 5(a) and 5(b) where scanned by a 2D-galvoscanner at scan rate (100 Hz) over (5mmX5mm) area and recorded using a photon counter (Hamamatsu photon counter model number H7155-21). Noted that we conducted characterization as soon as we fed the ants such that most particles were expected to be in the head area especially in the ant's mouth and started to enter into the body. We have observed using tomography in our recent studies [23] that NPs entered mealworm and were quickly transferred through their guts. In this study we wanted to see if the laser system works on insects, fire ants which have hard shell and complicated geometry

Optics EXPRESS

of their heads which behave as a lens and pose challenges for the laser beam to focus and penetrate into the body .So we didn't carry on extended study of particles transfer into ants. The evidence of nanoparticles (chemical state) inside the body was proven by the tomography images shown in Fig. 6 in section 3.4. Furthermore, the effects of NPs on ants would be done to observe how insects behave once they were fed with NPs. Since this work focuses on the feasibility of the laser system, our goal (desire) is to see the particles through their body shells, in particular their head shells that are hard and thicker than other part of the body. We performed a signal to noise ratio (SNR) measurements during scanning the fire ants samples with 980 nm laser, and then found the SNR ratio is about(250/k.counts signal from the nanoparticles to 10/ k.counts from the fire ant body). We can attribute this high contrast images to the excellent quality of well crystallized nanoparticles which reveal strong upconversion luminescence, non-photobleaching, and non-blinking in water-based biological samples such as fire ants. The laser intensity was 8) $kW.cm^{-2}$ which might be considered unsafe for biological samples including insect. However, we didn't see any damage to the ant samples. Our experiment was carried out rather quickly and ants didn't show any damages or burning on their bodies after scanning with this specific laser power. Figures 5(a, inset) and 5(b, inset) presents a strong and clear upconversion luminescence (UCL) spectra with high signal to noise ratio of $Y_2O_3:Er^{+3},Yb^{+3}$ UCNPs in which the emission bands reveal strong green luminescence emission and weak red emission spectra corresponding to the erbium (Er^{+3}) radiative transitions form ($^2H_{11/2}$, $^4S_{3/2}$, and $^4F_{9/2}$) excited states to $^4I_{15/2}$ ground state. Interestingly, the upconversion luminescence spectra appeared to be slightly different, even though they are accumulated from the same particles, the size of the ants are not identical. This change could be attributed to the upconversion nanoparticles' temperature sensitivity, where UCNPs have been used in optical temperature sensing [28,29]. Especially, temperature in biological sample can be measured by calculating the ratio of (520 nm and 550 nm emission peaks) of UCNPs doped with erbium and using Boltzmann distribution [30]. $Y_2O_3:Er^{+3},Yb^{+3}$ UCNPs can be used to accomplish fast and cheap optical bio-imaging whose absolute accuracy can be directly validated with x-ray imaging when desired.

Optics EXPRESS

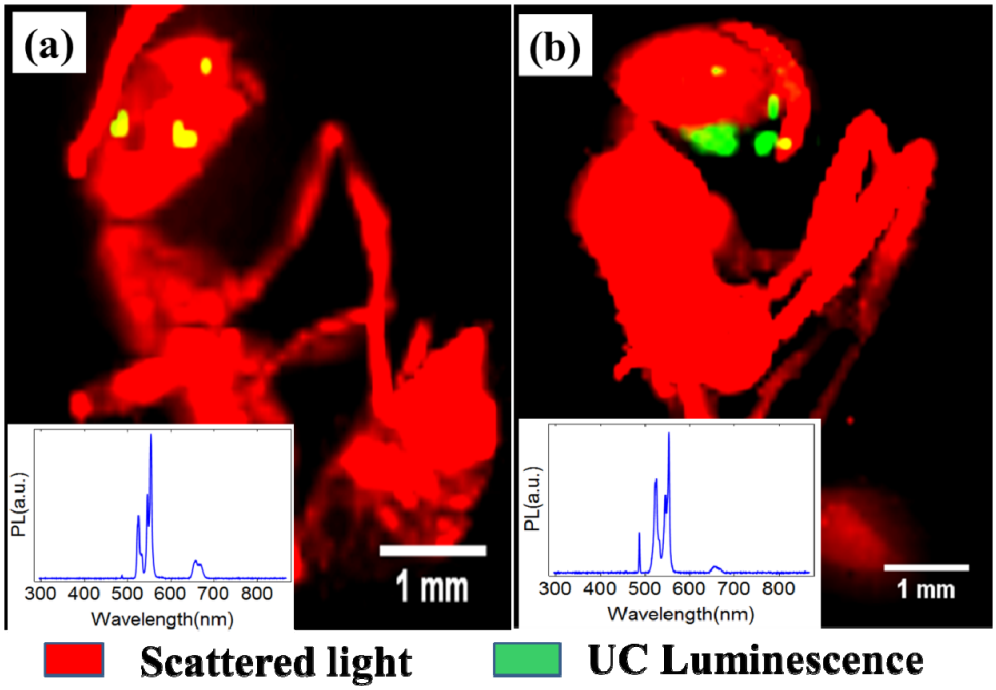

Fig. 5. (a) and (b) Upconversion imaging of fire ants fed with $Y_2O_3 : Er^{+3}, Yb^{+3}$ nanoparticles. These high contrast images were scanned by a 2D galvoscanner and emitted light collected by a photon counter. The inset presents photo luminescence (PL) spectra of the UCNPs in the green spots.

3.4 Conformation of imaging $Y_2O_3 : Er^{+3}, Yb^{+3}$ upconversion nanoparticles inside fire ants using synchrotron radiation micro X-ray computed tomography (SR-μXCT)

After achieving high contrast images of the UCNPs inside fire ants using an optical system, it was necessary to confirm that the nanoparticles are actually inside the body of the fire ants. Two fires ants from the same colony of southern fire ants were extracted and scanned using synchrotron radiation micro X-ray computed tomography (SR-μXCT). Details about this technique have been reported in our previous work [23, 31]. The locations of the upconversion nanoparticles inside the fire ants' body were confirmed by performing three dimensional X-ray imaging. The distribution of lanthanide-doped yttrium($Y_2O_3 : Er^{+3}, Yb^{+3}$ nanoparticles) within buccal cavity and anterior end of the digestive tract of the ant were segmented and marked in red as shown in Figs. 6(a) and 6(b).

Optics EXPRESS

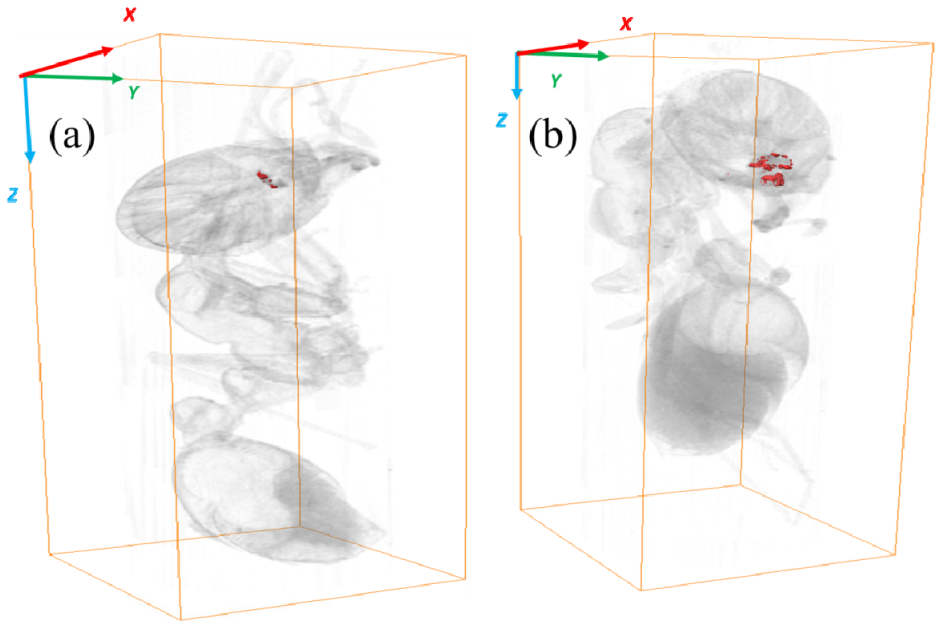

Fig. 6. (a) and (b). Three dimensional X-ray imaging of UCNPs inside two fire ants. The UCNPs inside the ant's body (ants' mouths) are segmented and marked in red. The size of frame box is 1.15 x 1.09 x 3.08 mm.

4. Conclusion

In conclusion, an economical and fast illumination optical system was designed for this experiment. We implemented $Y_2O_3:Er^{+3},Yb^{+3}$ nanoparticles as a bio-fluorescent probe in a small and challenging biological object such as southern fire ants. We accomplished high-contrast images of the upconversion nanoparticles locations inside the fire ants bodies. Results indicated that the high contrast images attributed to strong upconversion luminescence, water dispersibility, and photostability of $Y_2O_3:Er^{+3},Yb^{+3}$ nanoparticles. In addition, a strong up-conversion luminescence (UCL) with high signal-to-noise ratio from each red spot that represent UCNPs locations inside the fire ants was recorded. Thus, the locations of the UCNPs nanoparticles inside the ants' bodies were confirmed by x-ray tomography. This approach opens windows for future development in low-cost and highly effective detection systems. It also enables future investigation on the effects of nanoparticles on biological organisms that are crucial for protecting environments, managing pests, and detecting disease.

Funding

YYC was partially sponsored by the ALS fellowship. JMG was supported by the Provost's Assigned Time for Research (Summer 2016), and the California State University Fresno, Research, Scholarship and Creative proposal Award (2014-2016). JJP was supported by a CSUF Provost's Undergraduate Research award (2014 –2016). The Advanced Light Source is supported by the Director, Office of Science, Office of Basic Energy Sciences, of the U.S. Department of Energy under Contract No. DE-AC02-05CH11231. This work was partially sponsored by the Texas A&M Strategic Seed Grants program.